Monthly Notices
of the
ROYAL ASTRONOMICAL SOCIETY

MNRAS **431,** 1987–1994 (2013)
Advance Access publication 2013 March 15

doi:10.1093/mnras/stt315

Fast variability as a probe of the smallest regions around accreting black holes

Magnus Axelsson,[1,2]★ Linnea Hjalmarsdotter[3] and Chris Done[4]

[1]*Oskar Klein Center for CosmoParticle Physics, Department of Physics, Stockholm University, SE-106 91 Stockholm, Sweden*
[2]*Department of Astronomy, Stockholm University, SE-106 91 Stockholm, Sweden*
[3]*Sternberg Astronomical Institute, Moscow State University, Universitetskij pr. 13, 119899 Moscow, Russia*
[4]*Department of Physics, Durham University, South Road, Durham DH1 3LE, UK*

Accepted 2013 February 18. Received 2013 February 8; in original form 2012 December 22

ABSTRACT

We extract the spectra of the fastest variability (above 10 Hz) from the black hole XTE J1550−564 during a transition from hard to soft state on the rise to outburst. We confirm previous results that the rapid variability contains no significant disc component despite this being strongly present in the total spectrum of the softer observations. We model ionized reflection significantly better than previous work, and show that this is also suppressed in the rapid variability spectrum compared to the total emission. This is consistent with the fast variability having its origin in a hot inner flow close to the black hole rather than in the accretion disc or in a corona above it. However, the rapid variability spectrum is not simply the same as the total Comptonized emission. It is always significantly harder, by an amount which increases as the spectrum softens during the outburst. This adds to evidence from time lags that the Comptonization region is inhomogeneous, with harder spectra produced closest to the black hole, the same region which produces the fastest variability.

Key words: accretion, accretion discs – X-rays: binaries – X-rays: individual: XTE J1550−564.

1 INTRODUCTION

Spectral modelling is a powerful tool in understanding the physics of astrophysical sources including accreting black holes. By assigning observed/modelled spectral components to physical regions of the accretion flow we can learn about its geometry and how it changes as a response to changes in accretion rate.

The most popular physically motivated model for the X-ray spectra of accreting black holes is the combination of an accretion disc modelled as a multi-temperature blackbody and an inner hot flow and/or a corona above the disc, with hot electrons up-scattering the disc photons giving rise to a Comptonized component. Many spectra of black holes, especially in the soft/high to very high states, also require the presence of reflection of the Comptonized photons off some cooler material, presumably the accretion disc, and various lines, mostly from reflection and absorption from iron or other heavy elements. Such models of disc+Comptonization+reflection(+lines), modified by line-of-sight absorption, have been shown to rather successfully describe the spectra from black holes in a variety of spectral states at a range of accretion rates (for a review of spectra of black holes see Done, Gierliński & Kubota 2007).

In reality, however, inadequate models for the disc and reflection combined with poorly known parameters for Comptonization often make these components rather hard to separate, and spectral modelling therefore inherently suffers from degeneracy. In addition, more realistic modelling of the increasing amount of high-quality data often require more complexity than the 'basic' components. Especially for more complex models, a unique decomposition of the emission components may not be possible with spectral analysis alone, as there are many combinations which match a given observed spectrum.

Information about the accretion geometry may also be gleaned from analysis of temporal variability. The X-ray emission from black hole binaries is variable on time-scales from milliseconds to days. While the slower variations can be directly coupled to changes in the accretion rate, the source of rapid variability is more uncertain. Like the case with radiation spectra, there are likely several components to the variability. The broad-band variability is commonly studied through the power density spectrum (PDS). For black holes in the low/hard to intermediate (including so called very high) states the PDS can typically be well described by a combination of Lorentzian components (Belloni, Psaltis & van der Klis 2002) in the range 0.01–100 Hz, while the PDS during transitions into soft, strongly disc-dominated states is more variable and not easily decomposed. In addition to broad-band variability, many sources display quasi-periodic oscillations (QPOs), varying

★ E-mail: magnusa@astro.su.se

both with the spectral state of the source and the energy band being studied.

In this paper, we use the technique of frequency-resolved spectroscopy (Revnivstev, Gilfanov & Churazov 1999) to derive the (rms) energy spectrum of the variability. The significance of the rms energy spectrum is that it describes the energy spectrum of the process responsible for the variability, assuming the variability is generated by fluctuations in the normalization of a separate spectral component. The energy spectrum of the fast variability can then be directly compared to the continuum energy spectrum and help to constrain the observed components (e.g. Churazov, Gilfanov & Revnivtsev 2001; Revnivtsev & Gilfanov 2006; Sobolewska & Życki 2006).

2 XTE J1550−564

The transient black hole binary XTE J1550−564 was discovered on 1998 September 7 by the *RXTE* All-Sky Monitor (ASM; Smith 1998) and the *CGRO* Burst and Transient Source Experiment (BATSE; Wilson et al. 1998). This source has showed four subsequent outbursts since its discovery, but the first outburst remains the brightest and best covered by *RXTE* pointing observations. The data span nearly three decades in X-ray luminosity, capturing the source in each of the canonical states typically associated with black hole binaries. The broad-band spectrum of XTE J1550−564 has previously been modelled by several authors (e.g. Sobczak et al. 1999; Tomsick, Corbel & Kaaret 2001; Gierliński & Done 2003) including the data used here.

The variability of XTE J1550−564 is similar to that of other black hole binaries, and changes with the accretion rate. The PDS in the low/hard state is characterized by strong aperiodic noise. The total fractional variability is high, up to ∼30 per cent. The continuum of the power spectrum can usually be approximated as a broken power law with a flat power spectrum (in fP_f) between a low- and high-frequency break, and decreases at frequencies above and below these. The PDS evolves during the rising part of an outburst, with the low-frequency break moving to higher frequencies, with much less change at high frequencies (Psaltis, Belloni & van der Klis 1999; Gierliński, Nikołajuk & Czerny 2008). As the source enters a high/soft state, the power spectrum changes drastically, losing the low-frequency break (see e.g. Remillard et al. 1999). The amplitude of variability also decreases dramatically, but this is due to the increasing dominance of the stable disc component in the spectrum (Churazov et al. 2001).

XTE J1550−564 also exhibits transient high-frequency quasi-periodic oscillations (HFQPOs) as well as a stronger and more common low-frequency QPO (LFQPO; Cui et al. 1999; Remillard et al. 2002). The latter is seen to vary in frequency in response to changes in the radiation spectrum, coupled to variations in the accretion rate and geometry. In some observations a second low-frequency feature appears with harmonic content. Such a feature has also been seen in other black hole transient systems, e.g. GX 339−4 (Belloni et al. 2005).

3 DATA ANALYSIS

In this study we use archival data of XTE J1550−564 from the Proportional Counter Array (PCA; Jahoda et al. 1996) instrument onboard the *RXTE* satellite. The observations are made in the time period 1998-09-09 to 1998-09-16 (MJD 51065 to 51072) and cover the rise of the strong initial flare of the 1998 outburst (see Smith 1998, for more details on this outburst). We extracted Standard2 spectra for each observation applying standard selection criteria. A systematic error of 1 per cent was added to each bin in the spectra. This dominates over the statistical uncertainties, but we still use the standard $\Delta\chi^2 = 2.7$ to determine error ranges. The energy band used in the spectral modelling was 3–20 keV.

3.1 Spectral model

The data were fit in XSPEC using a spectral model comprising a disc blackbody, thermal Comptonization and Compton reflection. The disc component was modelled using DISKBB, where the main parameter is the maximum temperature T_{bb}. As our data only cover energies above 3 keV, far above the peak of the disc component, the disc temperature is poorly constrained so while we allow this to be free in the fits, we have to freeze it at the best-fitting value when calculating the error ranges for the other parameters.

For Comptonization we use the model NTHCOMP (Zdziarski, Johnson & Magdziarz 1996; Życki, Done & Smith 1999), parametrized by the asymptotic spectral index Γ, the seed photon temperature T_0 and the electron temperature kT_e. We set $T_0 = T_{bb}$ as can be expected if the seed photons are the photons from the disc. As it can be expected that the seed photons come from the inner edge of the disc, we choose a blackbody (rather than a disc spectrum) as the input type.

For Compton reflection we use RFXCONV. This is a convolution model that combines the reflected spectra of Ross & Fabian (2005) from a constant density ionized disc, with the IREFLECT convolution variant of the PEXRIV Compton reflection code by Magdziarz & Zdziarski (1995). The table models calculate the reflected spectrum and iron line from an X-ray illuminated slab including Compton up- and down-scattering below 12 keV but use a fixed spectral form (exponentially cut-off power law). By contrast, the IREFLECT model is a full convolution model for any continuum shape but neglects Compton scattering below 12 keV, has very approximate ionization balance and does not include the self-consistent iron line emission. The combination of these models into the new RFXCONV model thus allows us to model a physically much more correct reflection spectrum for the whole PCA energy range including a self-consistently calculated iron line. The RFXCONV model was demonstrated and briefly described in Kohlemainen, Done & Dìaz Trigo (2011) and is an updated version of the model first described in Done & Gierliński (2006). The main parameters are the relative amplitude of the reflected component, R, the inclination and the ionization parameter of the reprocessing matter, ξ.

We include photoelectric absorption, keeping the value of the column density frozen at $N_H = 0.6 \times 10^{22}$ cm^{-2} following the modelling in Gierliński & Done (2003). We also find that in all the data sets our fits are significantly improved by the addition of a narrow absorption line at ∼6.8 keV. Observations of similar strong absorption lines have been reported in several high-inclination Galactic binary systems and are believed to represent iron K resonance at 6.7 and 7.0 keV from outflowing material (e.g. Ueda et al. 1998, 2004; Kotani et al. 2000; Lee et al. 2002). Due to the limited resolution of the PCA data, we model the absorption line as a Gaussian of fixed (0.1 keV) intrinsic width. With the use of the RFXCONV model plus the absorption line our fits show virtually no residuals in the complex iron line region. Fig. 1 shows an example fit to one of the studied spectra using RFXCONV+GABS in comparison to the same data fitted with only RFXCONV and with IREFLECT+DISKLINE.

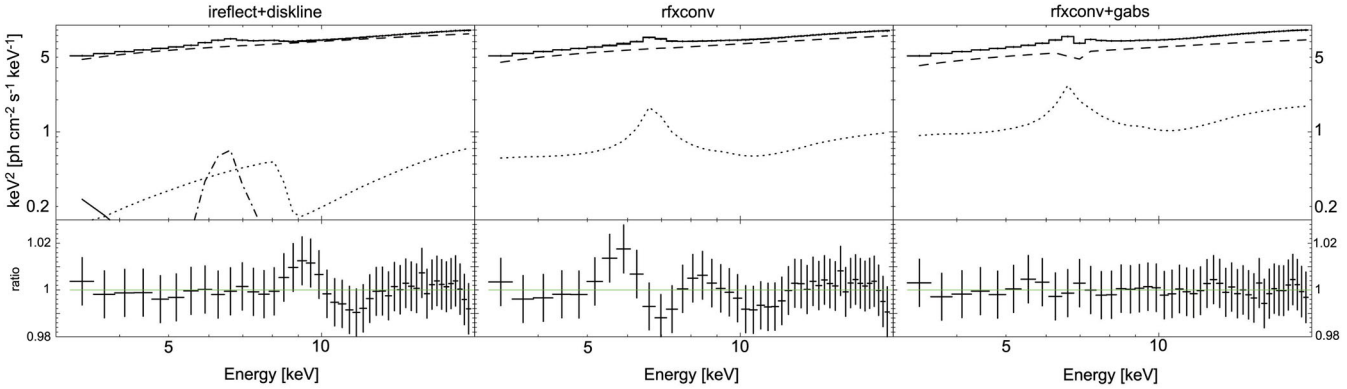

Figure 1. Fit to PCA data for spectrum 30188-06-01-00 with residuals, showing the results when using different models for the reflection. The dashed and dotted lines show the contribution from thermal Comptonization and Compton reflection, respectively. The models shown here are IREFLECT+DISKLINE (left-hand panel; dash–dot line shows the line component), RFXCONV (middle) and RFXCONV+GABS (right-hand panel). Although all fits are statistically very good (χ^2/d.o.f. < 0.5), the residuals clearly show that the region around the Kα iron line is not always well modelled. In this paper, we use RFXCONV+GABS, which provides the best model to the data.

3.2 Fourier spectroscopy

To compare the total spectrum to that of the rapid variability, we also performed frequency-resolved spectroscopy (Revnivstev, Gilfanov & Churazov 1999; Revnivtsev et al. 2001). Following the approach of Revnivtsev et al. (1999), we extracted a light curve for each available channel and constructed a PDS. By integrating the PDS over the frequency range of interest, we determined the relative contribution for each channel, and combined these to make an energy spectrum of the rapid variability. Throughout our observations, a strong QPO was present at $\leq$4 Hz, and a feature of harmonic content was seen in many observations as well, as reported earlier by Cui et al. (1999) and Remillard et al. (2002), among others. In order to avoid contamination from either the QPO or the harmonic, we chose the frequency range 10–50 Hz. As in the case of the Standard2 spectra, we added a 1 per cent systematic error.

Using the same technique, we also extracted the energy spectrum of the QPO. To obtain its contribution in each energy band, we fit the QPO feature in the PDS using a Lorentzian function, and integrate over this component (see also Sobolewska & Życki 2006). This gives a more accurate measure of its contribution than simply integrating the PDS over the energy range where the QPO dominates.

4 RESULTS

4.1 The total PCA spectra

In the first step, we fit the PCA Standard2 spectra with our model TABS×GABS×(DISKBB+NTHCOMP+ NTHCOMP×RFXCONV). For all spectra we find a very good fit, with χ^2/d.o.f. < 0.3 showing that the systematic error of 1 per cent dominates the statistical errors. The residuals clearly show that our improved model for the reflection matches the data very well. In particular, we note that our use of RFXCONV plus the absorption line enables us to make a good fit in the difficult region around the iron line, something which has proven difficult using earlier available models (e.g. Done & Kubota 2006).

Despite the limited bandwidth at low energies of the PCA, our model gives very reasonable, although not very well constrained, disc temperatures in the range of 0.5-0.7 keV, typical for intermediate/very high states. We note that the reason we are able to constrain the disc temperature at all is that we are using it as the seed photon temperature. Changing the disc temperature thereby affects also the Comptonized component of the spectrum. The asymptotic spectral index Γ increases from 1.8 in the hardest states to 2.4 in the softest. The electron temperature in our fits, 9–15 keV, is significantly lower than expected for the hard spectral states, where more typical temperatures are around 100 keV (e.g. Ibragimov et al. 2005; Torii et al. 2011). However, complex spectra with lower rollover temperatures are seen during transitions (Gierliński & Done 2003). Clearly, data extending to higher energies are required to constrain the electron temperature (as well as any possible existence of non-thermal Comptonization, which is not considered in our model).

Reflection is significantly detected in all spectra, with solid angle between 0.4 and 0.7, increasing with Γ as expected as the disc reaches further into the hot flow in the softer states (Revnivtsev et al. 2001). The ionization parameter of the reflector is rather high, around $\log \xi = 2.8$, and subsequently the peak of the iron line complex falls around 6.7 keV. The absorption line energy varies between 6.8 and 7.0 keV, consistent with resonant iron K resonance energies for this low-resolution data.

4.2 The spectrum of the variability

We now add the spectra of the rapid variability to the fit. We initially keep all parameters for both spectra frozen to the best-fitting values found for the PCA data alone, with the exception of the normalizations of the disc blackbody and the Comptonized component as well as the amplitude of reflection, which we allow to vary between the continuum and variability spectra. In the harder observations, this allows for an adequate fit also to the rms spectrum. However, as the spectrum evolves and becomes softer, it is no longer possible to find a good fit. We therefore allow also the asymptotic spectral index Γ to be different in the rms spectrum. This allows us to find good fits to all data sets. Table 1 shows the resulting parameter values. A decomposition of the fits to two of the data sets, ObsIDs 30188-06-01-02 and 30188-06-09-00, showing the spectral components is plotted in Fig. 2.

The most obvious difference between the continuum and the spectrum of the fast variability is in the strength of the blackbody and the reflection component. While the continuum spectra in all but the hardest states require a rather strong blackbody component, the data require that the normalization of this component is set

Table 1. Fit results for the model TBABS×GABS×(DISKBB+NTHCOMP+NTHCOMP×RFXCONV). Errors indicate 90 per cent confidence intervals.

ObsID	T_{bb} (keV)	N_{bb}	Γ	kT_e (keV)	R	E_{line} (keV)	EW ($\times 10^{-2}$ keV)	$\log \xi$	χ^2/d.o.f.	Flux erg cm^{-2} s^{-1}
30188-06-01-00	$0.56^{+0.31}_{-0.26}$	200^{+570}_{-200}	$1.77^{+0.03}_{-0.10}$	$14.8^{+7.3}_{-3.0}$	$0.44^{+0.12}_{-0.11}$	$6.84^{+0.11}_{-0.11}$	$9.5^{+4.0}_{-2.7}$	$2.80^{+0.03}_{-0.09}$	2.3/36	4.4×10^{-8}
rms			$1.69^{+0.03}_{-0.03}$		$0.07^{+0.09}_{-0.07}$				17.4/54	
30188-06-01-01	$0.55^{+0.04}_{-0.04}$	260^{+590}_{-260}	$1.80^{+0.03}_{-0.04}$	$15.1^{+5.8}_{-3.0}$	$0.43^{+0.14}_{-0.11}$	$6.85^{+0.09}_{-0.09}$	$9.2^{+3.5}_{-3.6}$	$2.80^{+0.67}_{-0.09}$	7.0/36	4.0×10^{-8}
rms			$1.66^{+0.09}_{-0.08}$		$0.06^{+0.25}_{-0.06}$				50.8/54	
30188-06-01-02	$0.55^{+0.28}_{-0.08}$	410^{+1100}_{-410}	$1.89^{+0.02}_{-0.02}$	$10.6^{+2.4}_{-1.5}$	$0.56^{+0.15}_{-0.14}$	$6.83^{+0.10}_{-0.09}$	$11^{+5.0}_{-4.7}$	$2.78^{+0.60}_{-0.09}$	4.5/36	4.3×10^{-8}
rms			$1.78^{+0.03}_{-0.03}$		$0.0^{+0.07}_{-0.0}$				35.2/54	
30188-06-01-03	$0.53^{+0.25}_{-0.09}$	970^{+1100}_{-970}	$1.94^{+0.03}_{-0.09}$	$10.9^{+2.3}_{-1.6}$	$0.52^{+0.15}_{-0.16}$	$6.80^{+0.08}_{-0.08}$	$9.6^{+2.5}_{-3.7}$	$2.78^{+0.70}_{-0.08}$	7.0/36	4.4×10^{-8}
rms			$1.79^{+0.03}_{-0.05}$		$0.07^{+0.21}_{-0.07}$				17.8/54	
30188-06-04-00	$0.53^{+0.19}_{-0.53}$	4100^{+1200}_{-2000}	$2.03^{+0.03}_{-0.03}$	$9.9^{+1.7}_{-0.7}$	$0.54^{+0.17}_{-0.15}$	$6.82^{+0.09}_{-0.09}$	$9.6^{+2.9}_{-3.9}$	$2.79^{+0.68}_{-0.05}$	6.1/36	5.1×10^{-8}
rms			$1.90^{+0.03}_{-0.03}$		$0.33^{+0.12}_{-0.11}$				38.9/54	
30188-06-05-00	$0.58^{+0.08}_{-0.58}$	8400^{+880}_{-2800}	$2.19^{+0.07}_{-0.04}$	$11.6^{+3.3}_{-1.4}$	$0.54^{+0.20}_{-0.17}$	$6.81^{+0.10}_{-0.11}$	$9.0^{+3.9}_{-2.9}$	$2.81^{+0.18}_{-0.22}$	6.0/36	6.0×10^{-8}
rms			$2.01^{+0.03}_{-0.03}$		$0.10^{+0.10}_{-0.10}$				28.2/54	
30188-06-06-00	$0.65^{+0.08}_{-0.45}$	9100^{+540}_{-1000}	$2.33^{+0.06}_{-0.06}$	$11.5^{+4.5}_{-1.5}$	$0.70^{+0.19}_{-0.20}$	$6.80^{+0.08}_{-0.09}$	$11^{+2.7}_{-3.7}$	$2.75^{+0.17}_{-0.16}$	5.6/36	5.4×10^{-8}
rms			$2.07^{+0.02}_{-0.04}$		$0.30^{+0.25}_{-0.13}$				38.7/54	
30188-06-07-00	$0.70^{+0.07}_{-0.51}$	6600^{+350}_{-560}	$2.27^{+0.08}_{-0.06}$	$10.4^{+2.7}_{-1.0}$	$0.64^{+0.15}_{-0.20}$	$6.81^{+0.08}_{-0.08}$	$11^{+3.0}_{-3.4}$	$2.78^{+0.23}_{-0.22}$	6.3/36	6.4×10^{-8}
rms			$2.11^{+0.03}_{-0.03}$		$0.29^{+0.08}_{-0.11}$				35.8/54	
30188-06-08-00	$0.70^{+0.07}_{-0.62}$	6500^{+310}_{-700}	$2.26^{+0.07}_{-0.15}$	$10.3^{+3.4}_{-0.84}$	$0.61^{+0.20}_{-0.16}$	$6.82^{+0.09}_{-0.08}$	$11^{+3.7}_{-3.8}$	$2.83^{+0.60}_{-0.13}$	5.4/36	6.4×10^{-8}
rms			$2.08^{+0.03}_{-0.03}$		$0.16^{+0.09}_{-0.09}$				47.0/54	
30188-06-09-00	$0.66^{+0.08}_{-0.45}$	9600^{+480}_{-900}	$2.39^{+0.08}_{-0.05}$	$12.8^{+5.3}_{-1.9}$	$0.67^{+0.16}_{-0.20}$	$6.79^{+0.08}_{-0.08}$	$9.5^{+3.0}_{-3.1}$	$2.73^{+0.14}_{-0.16}$	6.4/36	6.7×10^{-8}
rms			$2.08^{+0.03}_{-0.03}$		$0.22^{+0.13}_{-0.12}$				21.8/54	
30188-06-10-00	$0.52^{+0.12}_{-0.46}$	17000^{+3500}_{-4400}	$2.25^{+0.05}_{-0.04}$	$11.8^{+4.1}_{-2.1}$	$0.54^{+0.27}_{-0.14}$	$6.82^{+0.11}_{-0.12}$	$8.1^{+4.1}_{-4.0}$	$2.80^{+0.17}_{-0.10}$	8.2/36	6.2×10^{-8}
rms			$2.09^{+0.04}_{-0.04}$		$0.33^{+0.15}_{-0.13}$				34.3/54	
30188-06-11-00	$0.70^{+0.06}_{-0.33}$	8600^{+380}_{-750}	$2.40^{+0.08}_{-0.07}$	$11.9^{+4.1}_{-2.1}$	$0.65^{+0.24}_{-0.17}$	$6.79^{+0.09}_{-0.09}$	$11^{+3.4}_{-3.6}$	$2.78^{+0.22}_{-0.18}$	3.6/36	7.3×10^{-8}
rms			$2.15^{+0.03}_{-0.06}$		$0.16^{+0.22}_{-0.08}$				24.7/54	

to zero in the variability spectrum. The same is true for Compton reflection, which varies between 0.4 and 0.7 for the continuum, but is lower than 0.3 for all the spectra of the fast variability and in the cases with harder spectra consistent with zero reflection. (The ionization level of the reflector cannot be constrained for the low levels of reflection in the fast variability spectrum.) There are thus no signs of a disc in the spectrum of the fast variability, from either its direct or reflected emission.

Further, we note that Γ in all cases is harder in the rms spectrum than in the corresponding continuum spectrum. This shows that the fast variability has its origin in a separate Comptonization region where the plasma is more photon starved than for the overall Comptonization in the source. We note that we keep the electron temperature of the fast variability component frozen to the value for the continuum for simplicity since the fast variability spectrum is even more poorly constrained at higher energies than the continuum PCA data. To examine possible differences in the electron temperature or distribution between the origin of the fast variability and the continuum, both higher energy data and a more physical spectral model are required. However, our results already clearly show that the Comptonization region itself is inhomogenous. The rms spectra enable us to separate out the region where the fastest variability arises, and this region clearly sees less seed photons than the flow as a whole to produce its harder spectrum.

The differences between the rms and continuum spectra are highlighted in Fig. 3. The figure contrasts the behaviour of the disc blackbody, reflection and spectral index of the two spectra. As the rms spectra do not require any blackbody component, the upper limits are plotted against the strength of the blackbody as would be expected if simply scaling down the continuum spectrum (left-hand panel of Fig. 3). When the continuum spectrum is hard, the disc blackbody is not significantly detected in the time-averaged spectrum so we do not plot these points as they give no constraints. However, in the softer states when the disc component becomes more dominant, the upper limits from the rms spectra clearly rule out any correspondingly strong blackbody in the rms spectra. The two other panels in Fig. 3 directly compare the strength of reflection (middle panel) and spectral index (right-hand panel) derived from the fits.

Another striking result from our analysis is the apparent stability of the variability spectrum, despite the fact that the source changes state as evidenced by the large differences in the Standard2 spectra. While the Standard2 spectra change considerably with the spectral index Γ varying between 1.77 and 2.40, the shape of the variability spectrum varies between 1.66 and 2.15. This is clearly illustrated in Fig. 4 where we show Standard2 spectra from the whole time interval (upper panel) and the corresponding variability spectra (lower panel). The rms spectrum is thus less sensitive to a changing accretion rate and to a changing influx of soft photons.

4.3 Relation between fast variability and QPO

Previous studies have looked at the spectrum of the QPO in both XTE J1550−564 and other sources (Sobolewska & Życki 2006). In order to compare the rms spectrum to that of the QPO, we have extracted the spectrum of the latter as described in Section 3.2.

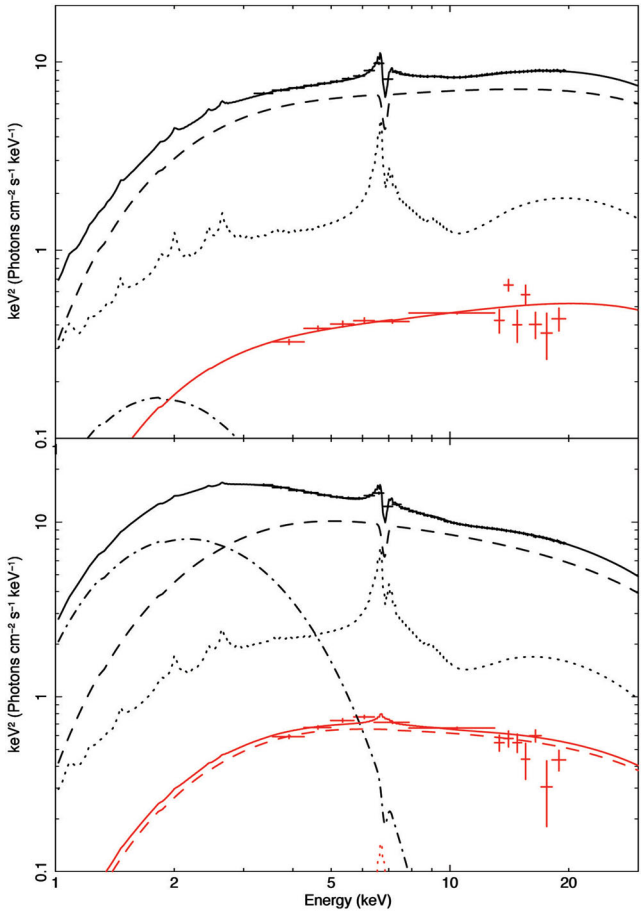

Figure 2. Example spectra (data and model components) from XTE J1550−564. The solid black spectrum shows a fit to the total continuum 3–20 keV PCA spectrum. The black dashed lines represent the Comptonized component, the dotted line the reflection and the dot–dashed line the disc blackbody, only required in the softer states (lower panel). The lower-normalization red spectrum shows a fit to the spectrum of the fast variability. This spectrum requires less reflection and does not require any thermal (blackbody) component.

In Fig. 5 we show a spectral fit to the PCA spectrum (left-hand column), the PDS from the observation (middle column) and the energy spectrum of the rapid variability (right-hand column). The two rows correspond to ObsIDs 30188-06-01-02 (top) and 30188-06-08-00 (bottom), respectively. The right-hand column also shows the spectrum of the QPO.

It is clear that the QPO spectrum is quite similar to that of the rapid variability (see also the neutron star spectra in Revnivtsev & Gilfanov 2006). This would be expected if both originate in a common physical region. There is perhaps a hint that the variability spectra turn down more sharply towards lower energies, but our data do not allow us to test whether this is a real effect. We note that the close similarity between the spectra ensures that any possible contribution from the QPO, despite our conservative limit of 10 Hz does not affect the shape of the rapid variability spectra.

The rms spectra of the QPO were modelled in detail by Sobolewska & Życki (2006). In contrast to the approach here, they used reflection models to fit the shape of these spectra. However, our more sophisticated reflection models clearly show that there is very little reflection in the fast variability spectra, hence it seems likely that the QPO rms spectra are similarly from Comptonized emission rather than reflection.

5 DISCUSSION

It has long been clear that the accretion flow is inhomogeneous, with components from a disc and corona. However, our results point to inhomogeneity also within the coronal emission itself, with different Comptonization spectra produced in different regions of the flow (see also Revnivstev, Gilfanov & Churazov 1999; Veledina, Poutanen & Vurm 2013).

This is particularly evident in the softer observations. The time-averaged spectra clearly show strong reflection and a strong disc component in addition to the Comptonization continuum. The fast variability spectrum lacks the reflection and direct disc emission, showing that the variability arises in a region of the corona where the disc subtends a small solid angle. However, the fast variability spectrum is not simply that of the time-averaged Comptonization spectrum, as would be expected if the corona was homogeneous. Instead, the fast variability spectrum is harder than the time-averaged Comptonization continuum. The variable part of the spectrum thus does not represent the whole Comptonized region, only a part of it, and the Comptonized component we see in the time-averaged spectrum cannot represent one uniform region but rather a superposition of at least two regions (one variable at high frequencies and one not). The different hardness and absence of reflection points to the variable part being physically separated from the other Comptonized region/regions (see also Yamada et al. 2013).

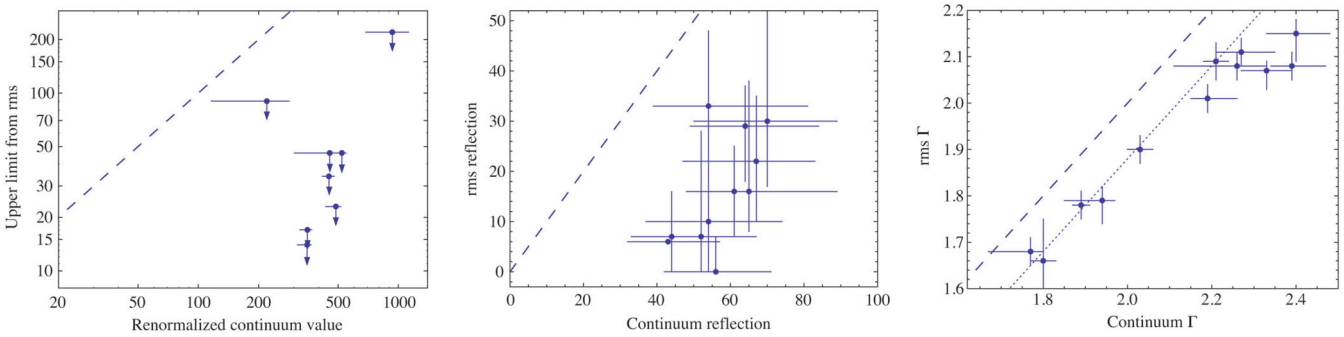

Figure 3. Comparison of disc blackbody (left-hand panel), amount of reflection (middle panel) and spectral index Γ (right-hand panel) between the continuum and variability spectra. In all panels, the dashed line shows where the two are equal. As the rms spectra do not require any blackbody component, the left-hand panel shows upper limits plotted against the strength of the blackbody that would be expected if simply scaling down the continuum spectrum to the level of the rms spectrum.

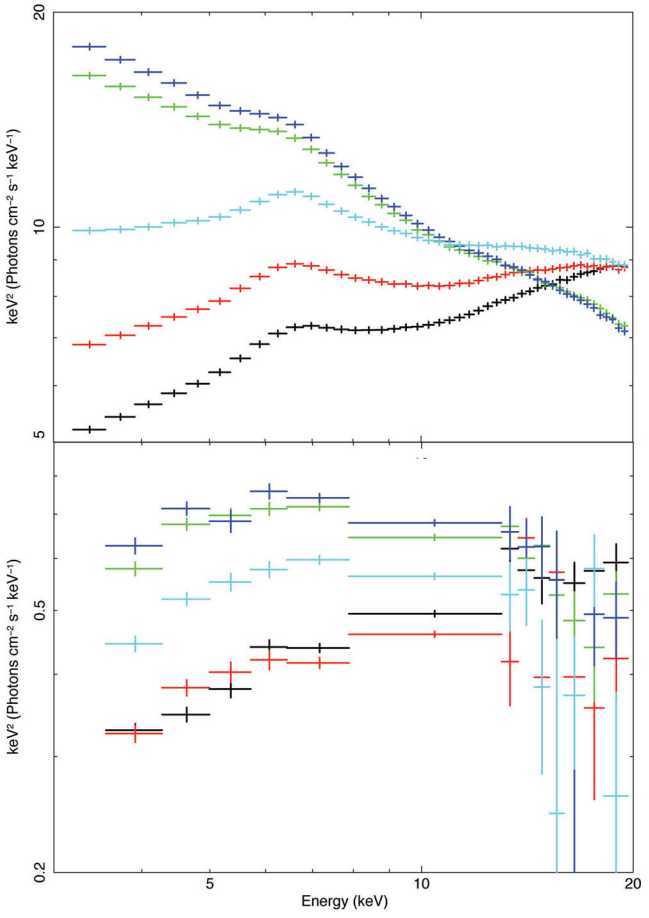

Figure 4. Sample of PCA (upper panel) and rms (lower panel) spectra used in this study. Although the PCA spectrum changes considerably, the spectrum of the rapid variability shows much less alteration.

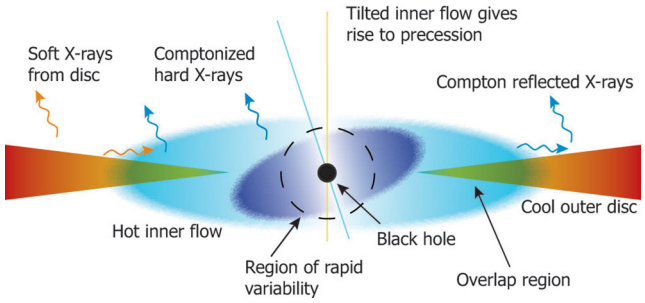

Figure 6. Sketch of accretion geometry with different emission regions indicated. Our results indicate that the region of rapid variability sees very few disc photons, indicating that it is far away from the disc and close to the black hole.

This has an obvious geometric interpretation in the truncated disc/hot inner flow picture where the inner region of the flow intercepts fewer seed photons from the disc (thus has a harder spectrum) than the outer regions which are closer, or even over the disc. In Fig. 6 we sketch a picture of our preferred geometry and origin of the fast variability (see also Yamada et al. 2013). This framework also explains the observed hard time lags seen in black hole binary systems (see e.g. Miyamoto & Kitamoto 1989). If the variability arises in the outer (softer) regions of the flow, and propagates inwards where the hard emission is produced, such lags are naturally produced (Kotov et al. 2001; Arévalo & Uttley 2006). We note that these lags will introduce decoherence, and so suppress variability on the time-scale of the lag (Focke, Wai & Swank 2005). However, Cui et al. (2000) show that the time lags in XTE J1550−564 are below a few milliseconds at frequencies above 10 Hz so this effect will be small.

The differences between continuum and fast variability rms spectra are not as great in the harder observations. However, better signal-to-noise ratio observations of Cyg X-1 reveals similar behaviour in the hard states also (Revnivtsev et al. 1999). Since the time lags are also present in these states (see, e.g. Miyamoto &

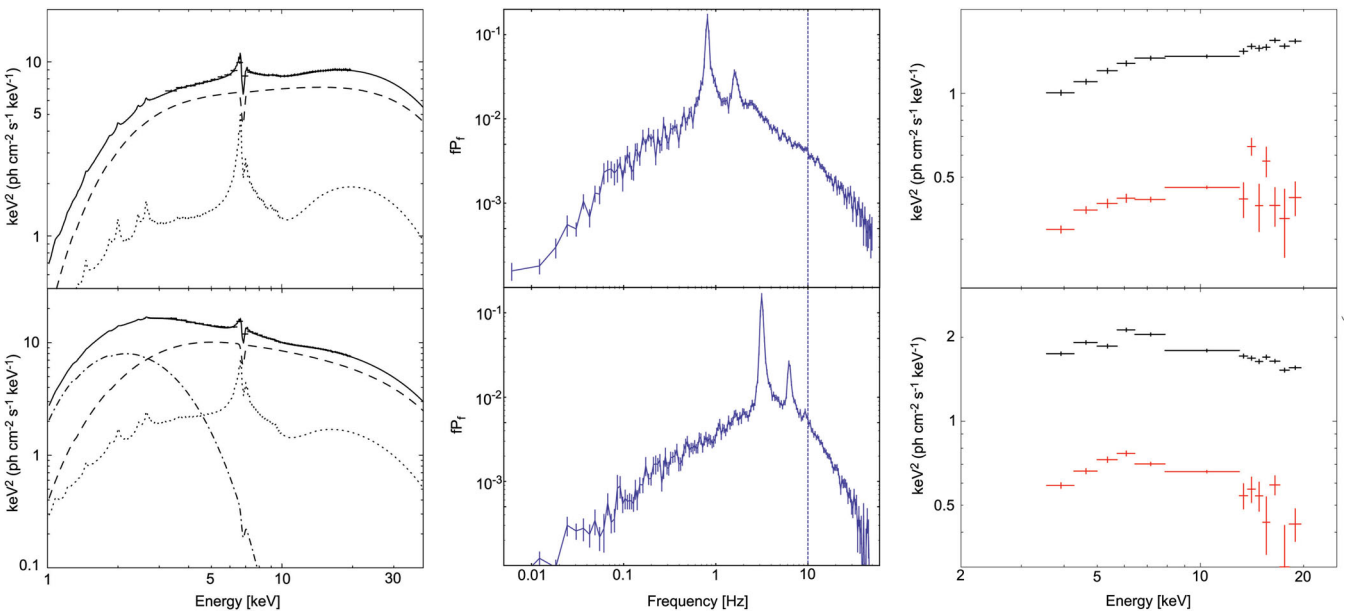

Figure 5. Fit of PCA spectra to our model (left-hand panels), the PDS of the observation (middle panels) and spectra of rapid variability and QPO (right-hand panels, QPO spectrum in black) for the observations 30188-06-01-02 (upper row) and 30188-06-08-00 (bottom row). The vertical line in the middle panels shows the 10 Hz lower boundary for the rapid variability spectra.

Kitamoto 1989; Torii et al. 2011) then the flow geometry is likely inhomogeneous here as well.

In the geometry of Fig. 6, the rapid variability is connected to a separate component, giving a straightforward interpretation of our results. However, this may not be unique. There is an alternative model involving spectral evolution of a single, homogeneous source (a magnetic flare whose Comptonized spectrum evolves from soft to hard as the flare rises above the disc) which also produces the observed time lag behaviour (Poutanen & Fabian 1999). Clearly, in this scenario the fast variability spectrum does not imply a separate component. However, we note that this specific model does not appear to match all aspects of the data. While they do not explicitly show an rms spectrum, it is clear that the model leads to spectral pivoting around 10–15 keV for their model parameters (a hard state), so there should be a minimum in the variability spectrum at this energy [as also shown by the power spectrum at 27 keV having less high frequency variability than that at 3 keV: fig. 2(a) of Poutanen & Fabian (1999)]. By contrast our data show that this is not the case, rather, we see a peak in variability in this energy band.

5.1 Spectral evolution

Our interpretation of an inhomogeneous geometry is also consistent with the observed long-term spectral evolution seen in the data. The source starts in the low/hard state, where the disc is truncated further from the black hole, then the spectra get softer and the direct disc and reflection components get stronger as the inner radius of the truncated disc moves in towards the black hole as the mass accretion rate increases.

The variability spectra also show some spectral evolution, but much less than seen in the time-averaged spectra. The fast variability spectrum is thus less sensitive to the increase in seed photons than is the total spectrum. Assuming a spherical geometry for the hot inner flow, purely geometrical considerations reveal that the fraction of disc photons intercepted by the flow interior to the disc truncation radius does not depend on the radius of the sphere (as long as it tracks the evolution of the inner disc radius). Therefore, even if the total spectrum will change dramatically in response to variations in accretion geometry, the energy spectrum of the rapid variability – if connected to the hot innermost flow – will retain a more or less constant ratio between the power supplied to the electrons and the power in the soft seed photons throughout the evolution.

5.2 Connection to the QPO

Recently, Ingram & Done (2011, 2012) presented the first physical model for creating broad-band variability and QPOs in the framework of the disc truncation scenario. They showed that propagating mass accretion rate fluctuations in the hot flow can match the broad-band power spectral properties seen. They also model the QPO as a vertical precession of the same inner part of the hot inner flow (see Fig. 6). The fact that the QPO and rapid variability have very similar spectra support this picture as a vertical precession can only occur for regions inside the disc truncation radius. The precessing region can thus only be interior to the disc truncation radius, so is associated with the same radii as produce the fastest variability. This predicts that the QPO spectrum also has little contribution from the disc and reflected emission. We will test this directly in a future paper (Axelsson et al., in preparation).

6 SUMMARY AND CONCLUSIONS

We have modelled the energy spectrum of the fast variability (10–50 Hz) in the Galactic black hole binary XTE J1550−564 and compared it to the time-averaged PCA continuum. We find that the spectrum of the rapid variability differs from the time-averaged continuum in that it requires no thermal disc component, is significantly harder and shows much less or no Compton reflection. The spectrum of the fast variability also shows less evolution of its spectral shape with increasing accretion rate than the time-averaged continuum. We conclude that the rapid variability arises in a hot inner flow close to the black hole, a region which does not intercept a large amount of seed photons from the disc. Thus it is not strongly affected by the increase of soft seed photons following a change in the geometry of the accretion flow in the transition from a hard to a very high state. The region is likely to collapse once the source enters a classical soft state, with the inner disc radius reaching all the way into the last stable orbit.

The fact that the spectrum of the fast variability differs from the continuum even after removing the blackbody and reflection components further suggests that the optically thin emission usually modelled as one single Comptonization component is likely a superposition of two or more components – one variable at high frequencies and one not. This shows the need for more complex models of the total spectra of black hole binaries in general.

ACKNOWLEDGEMENTS

This work was supported by The Royal Swedish Academy of Sciences and The Swedish Research Council (VR 623-2009-691). LH acknowledges support from the Wenner-Gren Foundations. CD would like to acknowledge useful discussions with Adam Ingram and Alex Smith. This research has made use of data obtained through the High Energy Astrophysics Science Archive Research Center (HEASARC) Online Service, provided by NASA/Goddard Space Flight Center.

REFERENCES

Arévalo P., Uttley P., 2006, MNRAS, 367, 801
Belloni T., Psaltis D., van der Klis M., 2002, ApJ, 572, 392
Belloni T., Homan J., Casella P., van der Klis M., Nespoli E., Lewin W. H. G., Miller J. M., Méndez M., 2005, A&A, 440, 207
Churazov E., Gilfanov M., Revnivtsev M., 2001, MNRAS, 321, 759
Cui W., Zhang S., Chen W., Morgan E., 1999, ApJ, 512, L43
Cui W., Zhang S. N., Chen W., 2000, ApJ, 531, L45
Done C., Gierliński M., 2006, MNRAS, 367, 659
Done C., Kubota A., 2006, MNRAS, 371, 1216
Done C., Gierliński M., Kubota A., 2007, A&AR, 15, 1
Focke W. B., Wai L. L., Swank J. H., 2005, ApJ, 633, 1085
Gierliński M., Done C., 2003, MNRAS, 342, 1083
Gierliński M., Nikołajuk M., Czerny B., 2008, MNRAS, 383, 741
Ibragimov A., Poutanen J., Gilfanov M., Zdziarski A. A., Shrader C. R., 2005, MNRAS, 362, 1435
Ingram A., Done C., 2011, MNRAS, 415, 2323
Ingram A., Done C., 2012, MNRAS, 419, 2369
Jahoda K., Swank J. H., Giles A. B., Stark M. J., Strohmayer T., Zhang W. W., Morgan E. H., 1996, in Siegmund O. H. W., Gummin M. H., eds, Proc. SPIE Vol. 2808, EUV, X-Ray, and Gamma-Ray Instrumentation for Astronomy VII, SPIE, p. 59
Kohlemainen M., Done C., Dìaz Trigo M., 2011, MNRAS, 416, 311
Kotani T. et al., 2000, Adv. Space Res., 25, 445
Kotov O., Churazov E., Gilfanov M., 2001, MNRAS, 327, 799

Lee J. C., Reynolds C. S., Remillard R., Schulz N. S., Blackman E. G., Fabian A. C., 2002, ApJ, 567, 1102
Magdziarz P., Zdziarski A. A., 1995, MNRAS, 273, 837
Miyamoto S., Kitamoto S., 1989, Nat, 342, 773
Poutanen J., Fabian A. C., 1999, MNRAS, 306, L31
Psaltis D., Belloni T., van der Klis M., 1999, ApJ, 520, 262
Remillard R. A., McClintock J. E., Sobczak G. J., Bailyn C. D., Orosz J. A., Morgan E. H., Levine A. M., 1999, ApJ, 517, L127
Remillard R. A., Sobczak G. J., Muno M., McClintock J. E., 2002, ApJ, 564, 962
Revnivstev M., Gilfanov M., Churazov E., 1999, A&A, 347, L23
Revnivtsev M., Gilfanov M., Churazov E., 2001, A&A, 380, 520
Revnivtsev M. G., Gilfanov M. R., 2006, A&A, 453, 253
Ross R. R., Fabian A. C., 2005, MNRAS, 358, 211
Smith D. A., 1998, IAU Circ. 7008
Sobczak G. J., McClintock J. E., Remillard R. A., Levine A. M., Morgan E. H., Bailyn C. D., Orosz J. A., 1999, ApJ, 517, L121
Sobolewska M. A., Życki P. T., 2006, MNRAS, 370, 405
Tomsick J. A., Corbel S., Kaaret P., 2001, ApJ, 563, 229
Torii S. et al., 2011, PASJ, 63, 771
Ueda Y., Inoue H., Tanaka Y., Ebisawa K., Nagase F., Kotani T., Gehrels N., 1998, ApJ, 492, 782
Ueda Y., Murakami H., Yamaoka K., Dotani T., Ebisawa K., 2004, ApJ, 609, 325
Veledina A., Poutanen J., Vurm I., 2013, MNRAS, in press (arXiv:1210.0236)
Wilson C. A., Harmon B. A., Paciesas W. S., McCollough M. L., 1998, IAU Circ. 7010
Yamada S. et al., 2013, PASJ, in press
Zdziarski A. A., Johnson W. N., Magdziarz P., 1996, MNRAS, 283, 193
Życki P., Done C., Smith D. A, 1999, MNRAS, 309, 561

This paper has been typeset from a TEX/LATEX file prepared by the author.